Wireless Power and Bidirectional Data Transfer Scheme for Battery Charger

Chih-Cheng Huang and Chun-Liang Lin, *Senior Member, IEEE*

***Abstract*—Wireless battery charging has been becoming a recent trend in mobile devices. However, there are relatively less research efforts focusing on the large power applications. It is a major drawback of the battery charging in traditional electric vehicles which relies on the use of a plug-in charging device. This paper proposes a wireless power and bidirectional data transmission scheme, data related to battery status, vehicle identification number, or emergency messages that can be mutually transmitted between two isolated units via the same *LC* tank. The primary unit employs an inverter to yield alternating current and power flow to the load via mutual inductance. The secondary unit transfers data by adjusting current of load, and the primary unit receives data based on the zero-voltage switching method. The primary unit transfers command by trimming the current's curve and the secondary unit receives command and make decoding using the period of carrier wave. It is worth to mention that the design scheme enables it to handle the situation of emergency by sending back the message to the primary unit to make an emergency halt.**

***Index Terms*—Communication systems, electric vehicle, power and bidirectional data transmission, wireless power transfer, zero-voltage switching (ZVS) method.**

I. Introduction

INDUCTIVE power transfer (IPT) is designed to deliver power from a stationary primary source to one or more movable pickup units through mutual inductance magnetic coupling over an air gap. The wireless charging method becomes increasingly popular in industrial and domestic applications over a wide ranges [1], [2] recently leading to various utilizations such as contactless battery charging for electric vehicles [3]–[7], induction cooking heat [8], [9], bidirectional IPT [10]–[12], vehicle-to-grid power systems [13], [14], cell medical implants system [15], [16], phones charging [17], avionic applications system [18], dynamic charging systems [19], [20], power and data transfer system [21], [22], and special applications [23]–[26].

A survey of empirical wireless power transfer across diverse applications with different technologies was presented in [1] by comparing power level, gap distance, operational frequency, and efficiency. Wu *et al*. [2] presented a state of the art literature review on the recent advancements of IPT technology used in electric vehicle (EV) charging. However, most of the literature focus on power transfer alone. In [10], its proposed IPT system shows high operational efficiency and it has been applied to vehicle battery charging. In the system architecture, it consists of outer and inner control loops to handle the dual-side control strategy, which employs an added wireless communication device to transfer data from the secondary side to the primary side. However, considering better power transfer safety of two isolated units, it is necessary to keep monitoring battery status feedback to the primary unit at all times. In [22], the IPT system used contactless technology to transfer power and information transmission in a drill machine. It has two sets of coils for power and data transmission. However, the system works with two operating frequencies, which may result in relatively high cost in the products. Wang *et al.* [27] have proposed a method to detect load parameters in the IPT system that is important to establish an efficient and stable wireless power supply of good quality for cookroom appliances. A transient load detection method is to detect load parameters and loading conditions by utilizing the energy injection mode and free resonant mode to check the feedback signals for load information. This method is simple and reliable. However, it does not include the function of data transmission.

The work presented here proposes a completely new contactless power and bidirectional data transmission scheme using a flyback converter which utilizes zero-voltage switching (ZVS) method to improve power transfer efficiency and reduces electromagnetic interference (EMI) noise. The secondary unit modulates data by adjusting instantaneously the load current, and the primary unit receives data under ZVS. The primary unit sends command by trimming current and the secondary unit receives command and conducts data decoding. Sheikhian *et al*. [28] presented a transient load detection approach to detect load conditions alone by utilizing the energy injection and free resonant modes. Our approach possesses the similar structure; however, the focus and functions are completely different. Here, bidirectional digitized data transmission is considered.

The primary design motivated in this work intends to illustrate the structure of this effective power and bidirectional data transmission scheme which can be used with the vehicle positioning system serving as a wireless vehicle charge station. In addition to the vehicle positioning system for locating the optimal parking location for energy transmission in the parking lot, extra messages during battery charge can be involved. This may include vehicle identification number, battery status, emergency

Manuscript received January 20, 2017; revised June 9, 2017; accepted June 30, 2017. Date of publication July 11, 2017; date of current version February 22, 2018. Recommended for publication by Associate Editor R. Zane. *(Corresponding author: Chun-Liang Lin.)*

The authors are with the Department of Electrical Engineering, National Chung Hsing University, Taichung 402, Taiwan, R.O.C. (e-mail: erichuang2014@hotmail.com; chunlin@dragon.nchu.edu.tw).

Color versions of one or more of the figures in this paper are available online at http://ieeexplore.ieee.org.

Digital Object Identifier 10.1109/TPEL.2017.2725940

message, and information for miscellaneous applications. This paper mainly focuses on the development of the simultaneous power and bidirectional data transmission scheme. Design of the positioning system will come in another publication.

Novelty and merits of the proposed IPT system are summarized as follows:

1) the feature of bidirectional data communication via magnetic flux between induction coils possesses advantages such as no channel interference, no robust EMI, no need of complicated device settings, no base stations, and no robust to severe environmental condition;
2) the charging status (voltage and current) can be governed from the primary side (ground station);
3) the vehicle license ID can be recognized by the grid side for billing. This function is essential for applications of microgrid in a parking lot.

II. System Design

A. Circuit Design

In this work, a wireless vehicle charger with the capacity of simultaneous power and bidirectional data transferring scheme is studied. During startup, the primary unit in our design works with two tasks in order: payload detection and soft start (initial current generation). The former detects if there is payload at the secondary side. If there is no load on the pad's inductance, the primary unit will not output power. If a load detected, the soft-start current will be ramped up to a preset level. This mechanism had been used to minimize surge current flowing through the switch. The grid (primary) side plays as the power supply using the utility power source of ac 110 V/60 Hz.

The vehicle (secondary) side receives power transferred from the primary side to the vehicle battery. In addition to power delivery, both sides can transmit and receive message via the same conduction coils. Fig. 1 illustrates the schematic diagram of the proposed system. The system adopts a flyback inverter, which is constituted by ordinary electronic components which is also small in size for convenience of installation in engine compartment.

Referring to this figure, the system consists of two mutually magnetic coupling circuits. For the grid powered battery charging station, after converting the utility power to V_{bus} via a rectifier and filter, the transmitter generates power at the primary coil and induces mutually to the secondary coil within the vehicle to carry out the wireless power delivery. Q_2 at the secondary side has two functions, i.e., it bypasses output current and transmits the "*Tx* data" such as output voltage, current, etc. The primary side receives data by detecting the period of the feedback voltage V_c. A second-order low-pass filter formed by the inductances L_{01} and L_{02} and capacitors C_{21} and C_{22} is used to filter current variation resulting from data transmission during batter charge.

For data communication, after the *Tx* data have been received at the primary side, it will be acknowledged. Q_1 at the primary side reacts by sending a command back to the secondary side. In the secondary side, a current transducer is connected to the circuit to receive the command.

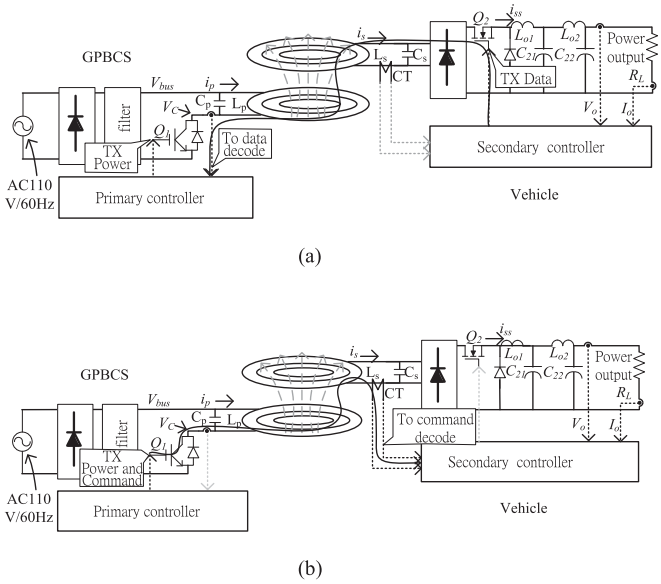

Fig. 1. Schematic diagram of the simultaneous wireless power and bidirectional data transfer system. (a) Signal transmission path of data feedback. (b) Signal transmission path of command sending.

At the primary unit, parameter tuning of the *LC* compensation circuit is essential. Though such tuning depends on the load, it is not necessary to adapt the resonant system because the coupling factor is low. The operational frequency is given by

$$f = \frac{1}{2\pi\sqrt{L_p C_p}} \tag{1}$$

where L_p and C_p are compensation inductance and capacitance at the primary unit, respectively.

B. Topologies

In the IPT systems, the open-circuit voltage (V_{OC}) and short-circuit current (I_{SC}) of the power pad, and the quality factor can be measured. Therefore, the power can be calculated by

$$P = P_{\text{SU}}Q = V_{\text{OC}}I_{\text{SC}}Q = \omega M I_p^2 \frac{M^2}{L_s}Q$$
$$= V_p I_p^2 k^2 Q \tag{2}$$

where ω is frequency of the current i_p, V_p is voltage across L_p., and P_{SU} is the uncompensated power rating. As shown in Fig. 1, the mutual inductance *M* is related to the magnetic coupling factor and the load quality factor *Q* of the secondary unit which are given by

$$k = \frac{M}{\sqrt{L_p L_s}} \tag{3}$$

$$Q = \omega C_s R_L \tag{4}$$

where L_p is measured with the transmitter pad presented but open circuit. The operational frequency and power rating of the supply are limited by the switching components that are presently available, and both have to be balanced based on the switching and copper losses. This work has selected suitable *Q*

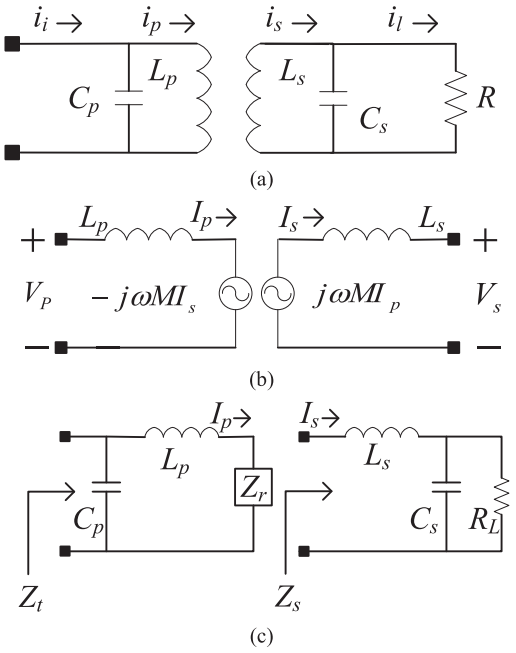

Fig. 2. (a) P-P type topology, (b) mutual inductance coupling circuit, and (c) equivalent impedance circuit.

and *k* to remain transfer power efficiency [7] and S/N ratio for controlling data transmission quality.

The simultaneous wireless power and bidirectional data transfer system adopts parallel–parallel (PP) reactive power compensation. The parallel-compensated primary unit is used to generate large primary current. The parallel-compensated secondary unit works like a current source in which the characteristics of the parallel secondary unit are appropriate for battery charging [5]. The simplified topology of PP-type compensation is illustrated in Fig. 2(a). By a mutual inductance coupling model, this topology can be modeled by the circuit illustrated in Fig. 2(b). The compensation network with equivalent impedance is illustrated in Fig. 2(c).

The voltages across the primary and secondary windings are given, respectively, by

$$V_p = -j\omega M I_s + j\omega L_p I_p \tag{5}$$

$$V_s = -j\omega M L_s I_s + j\omega M I_p. \tag{6}$$

The current flowing the secondary winding is given by

$$I_s = \frac{j\omega M I_p}{Z_s}. \tag{7}$$

Normally, the resonant frequencies of the primary and secondary sides are identical

$$\omega = \frac{1}{\sqrt{L_p C_p}} = \frac{1}{\sqrt{L_s C_s}}. \tag{8}$$

The respective impedances of the secondary unit is given by

$$Z_s = j\omega L_s + \frac{1}{j\omega C_s + \frac{1}{R}}. \tag{9}$$

The reflected impedance from the secondary unit to the primary unit is given by

$$Z_r = \frac{\omega^2 M^2}{Z_s}. \tag{10}$$

Data transmission from the secondary unit to the primary unit is conducted with the same mutual inductance. The load impedance at the primary side is determined by combining the primary and secondary networks, i.e.,

$$Z_t = \frac{1}{j\omega C_p + \frac{1}{j\omega L_p + Z_r}}. \tag{11}$$

To minimize VA rating, it is common to select imaginary components of the load impedance to be zero at the resonant frequency (ω_0) of the secondary side.

Substituting (9) into (10), the reflected resistance and reactance [3], [29] can be obtained as

$$Z_r = \frac{\omega_0^2 M^2}{Z_s} = \frac{M^2 R}{L_s^2} - j\frac{\omega_0 M^2}{L_s}. \tag{12}$$

Substituting (12) into (11), the load impedance can be obtained as

$$Z_t = \frac{1}{j\omega_0 C_p + \frac{L_s^2}{M^2 R + j(\omega_0 L_p L_s^2 - \omega_0 L_s M^2)}}. \tag{13}$$

This matches to the standard form as

$$Z_t = \frac{1}{ja + \frac{b}{c + jd}}. \tag{14}$$

Selecting the imaginary components of the load impedance Z_t to be zero as follows:

$$db - a\left(c^2 + d^2\right) = 0 \tag{15}$$

where

$$a = \frac{bd}{\left(c^2 + d^2\right)}. \tag{16}$$

From which we easily know that

$$C_p = \frac{\left(L_p L_s - M^2\right) C_s L_s^3}{M^4 C_s R^2 + L_s \left(L_p L_s - M^2\right)^2}. \tag{17}$$

C_p compensates not only the primary inductance, but provides the reflected impedance in series with the primary winding.

C. Power Pad

Two nominally identical circular magnetic structures are used as power pads to couple flux between the primary transmitter and secondary receiver. Both sides communicate through the power pads as well. Each power pad has four major components illustrated as in Fig. 3.

D. Measurement

The proposed system is supplied by a utility power source with 110 VAC 60 Hz. The measurement considers output power up to 700 W across the load R_L when no data are transferred.

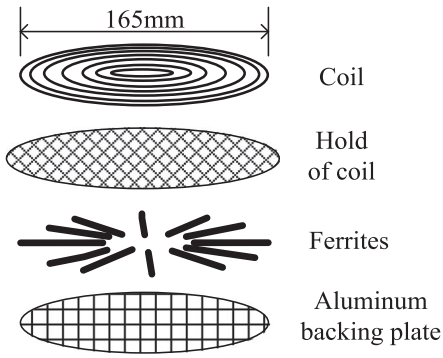

Fig. 3. Structure of the power transmission pad.

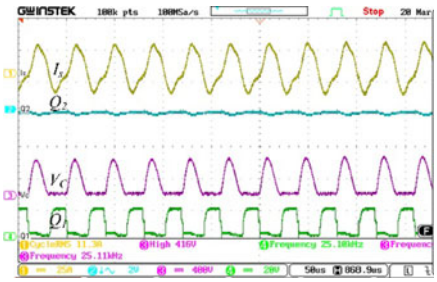

Fig. 4. Wireless 400 W power transfer (under 25 mm air gap and 0 mm offset).

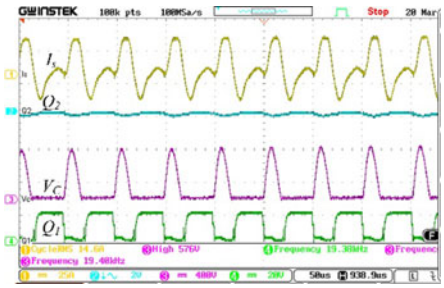

Fig. 5. Wireless 700 W power transfer (under 25 mm air gap and 0 mm offset).

In Figs. 4 and 5, the first curve represents I_s, the second curve represents the ON-OFF status of Q_2 with duty cycle 100%, the third curve represents V_c, and the last curve represents the gate voltage of Q_1. Q_1 turns ON when V_c reaches 0 V. When Q_1 turns OFF, both of V_c and I_s increase. This shows characteristics of the ZVS method.

III. Data Transmission

Simultaneous wireless power and bidirectional information transmission is a practical enhancement of the current wireless power charging device. With which, the vehicle identification number, battery status, active control commands, and many others could be mutually communicated via the system. We propose a data attached method to synchronize the carrier wave with the same *LC* tank. This is introduced below.

To prevent data collision, the data string is arranged as illustrated in Fig. 6 where reset time is set to wait for the next

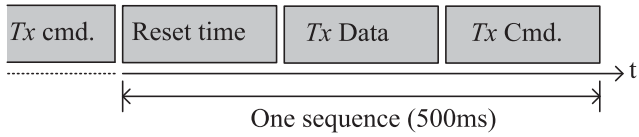

Fig. 6. Format of data sequence.

TABLE I
Protocol for Data Communication

Data type	Baud rate	Start segment	Data segment	Checksum segment	Stop segment
Normal	120 Bd.	1 bit	8 bit	8 bit	1 bit
Emergency	Operating freq. Bd.	1 bit	4 bit	4 bit	1 bit

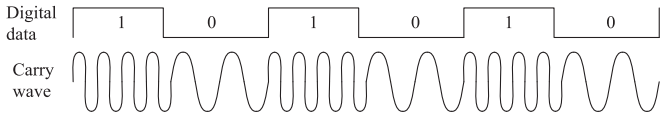

Fig. 7. BFSK technique.

string, "*Tx* data" refers to the feedback normal message from the secondary side such as output voltage, current, etc., and "*Tx* cmd" is sent from the primary side to command the secondary side for the corresponding action.

A. Communication Protocol

We divide data into two categories according to the attribute of the message sources to be transmitted. The first category is the normal message, such as output voltage, current, etc. It is processed with a slower rate. The *Tx* data of the secondary side are sent to the primary unit for charging efficiency calculation. The *Tx* cmd of the primary side is sent to the secondary side as a command issuer. The second category is the emergency message source, such as over voltage, over current, etc. It is processed with a faster data rate for prompt reaction. Specifications of the data packet for normal and emergency messages are summarized in Table I.

We use the frequency-shift keying (FSK) technique for data modulation with which digital information is transmitted through discrete frequency changes of a carrier wave to modulate data. The binary FSK (BFSK) adopts a pair of discrete frequencies to distinguish and transmit binary data (0 s and 1 s) as shown in Fig. 7. While transmitting power, we implement BFSK to the IPT system to transmit digital signal simultaneously. The binary system for the digital signal is defined as

$$s(t) = \begin{cases} A\cos(2\pi f_c t), & "1" \\ A\cos(2\pi f_z t), & "0" \end{cases} \tag{18}$$

where $s(t)$ is the carry wave, f_c is the working frequency representing the digital "1," and f_z is the frequency with which the IPT modulation refers to the digital "0." For details of the BFSK method, one is referred to [30].

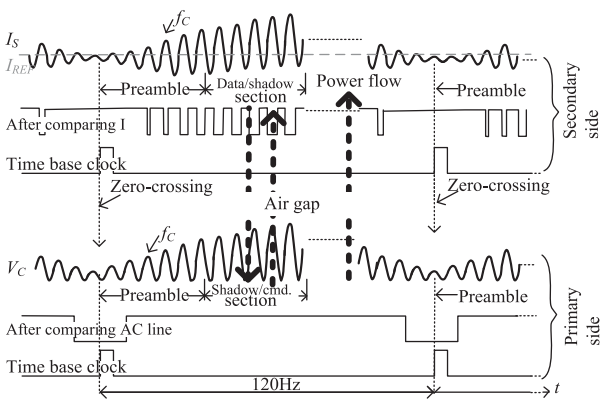

Fig. 8. Description of the bidirectional data transmission principle via two mutually magnetic coupling circuits.

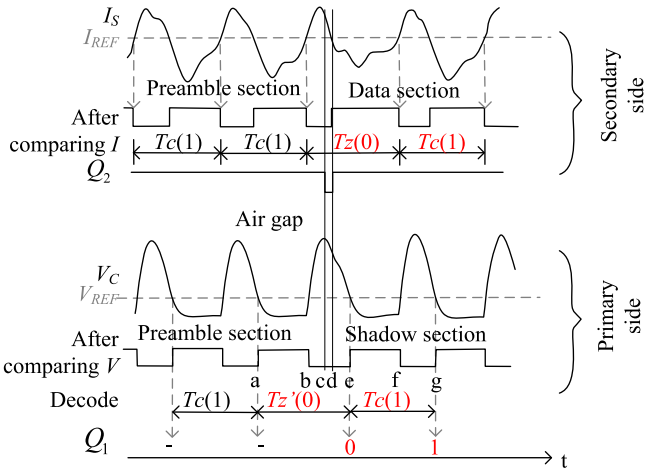

Fig. 9. Data transmission and decoding mechanism.

The primary unit transfers power to the secondary unit and data transmission communicates both sides as depicted in Fig. 8. In the figure, the period between zero-crossing is identical to that of the ac line. The primary unit employs a zero-crossing detection circuit to yield "after comparing ac line" signal as the time base clock. The secondary side uses a current sensor to measure I_s and make comparison to yield "after comparing I" signal. The processor utilizes it to generate the time-based clock as well.

The carry frequency f_c, measured during the preamble period on both sides, can be used to discriminate digital "0" or "1." In the preamble section, T_{OFF} of the duty cycle of Q_2 is fixed. The secondary unit sends data emerged in data section and the primary side receives data in the shadow section. When the primary unit places and sends command in the cmd section, the secondary side receives and places it in the shadow section.

B. Data Transmission

Fig. 9 pictures how the system transmits power to the load R_L and acquires information back simultaneously, in which V_{REF} and I_{REF} can be a fraction as opposed to V_c and I_s, respectively.

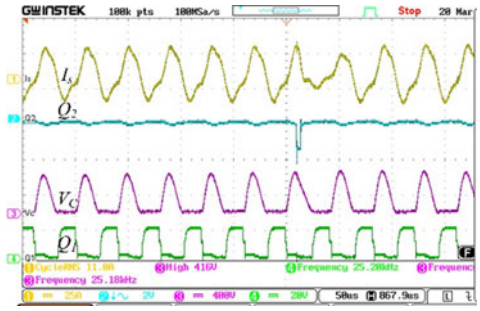

Fig. 10. Simultaneous wireless 400 W power transfer while simultaneously modulating a digit "0" by reducing the duty cycle of Q_2 from 100% to 94% (under 25 mm air gap and 0 mm offset).

The second curves of the primary and secondary sides are obtained from comparators. Here, $T_c(1)$ and $T_z(0)$ are derivatives of f_c and f_z, respectively. In the preamble section, both sides measure and calculate $T_c(1)$ with duty cycle of Q_2 equal to 100%.

In data section, the secondary unit arranges data sequence to be transmitted. When the data bit is $T_z(0)$ (with modulation), the output current is reduced by decreasing the duty cycle of Q_2. The reduced current produces a time delay $\Delta\tau$ at the secondary side. Referring to Fig. 9, in the c-d section, Q_2 is OFF, the current I_s flowing through the load R_L will store in C_s. During the d-e section, Q_2 is ON, C_s discharges to R_L. The delayed discharge of C_s will be affecting V_c at the primary unit [see (5)]. This delays the time of V_c reducing to 0 V, causing a bump at the falling part of V_c corresponding to the d-e section. Q_1 works under ZVS; thus, the time to turn ON Q_1 is delayed as well (at around the time point e). This induces an extra time delay $\Delta\tau$ in the a–e section while compared with that in the e–g section. The time delay $\Delta\tau$ generating the digital "0" is defined as

$$T_z(0) = T_c(1) + \Delta\tau \tag{19}$$

where $T_Z(0)$ (with modulation) is the period of the carrier wave for digit "0" and $T_C(1)$ (the normal status, i.e., without modulation) is for digit "1." $\Delta\tau$ refers to the S/N ratio. Increasing $\Delta\tau$ implies better robustness and data transmission quality against noises which would be beneficial for the controller at the primary side to decode signals.

As mentioned above, the secondary unit transmits digits "0" and "1" by $T_Z(0)$ and $T_C(1)$ in data section. The primary unit receives modulated data and decodes it to be "0" and "1" depending on $T_Z{}'(0)$ and $T_C(1)$. The principle for the primary unit distinguishes the digital "0" is based on the following formula:

$$T_Z{}'(0) > T_C(1) + \Delta\text{ref} \tag{20}$$

where Δref is a threshold for judging the digit "0" at the primary side. If $\Delta\tau > \Delta$ref, (20) holds. Figs. 10 and 12 display the function for modulating a digital "0"at the center of the data string. The first to the fourth curves represent, respectively, I_s, the ON-OFF status of Q_2, V_C and the gate voltage of Q_1. One can see $T_Z(0)$ by modulating the duty cycle of Q_2 from 100% to 94% in Figs. 10 and 11 for 400 and 700 W power transfer, respectively, and 90% to 80% in Fig. 12 for 350 W power

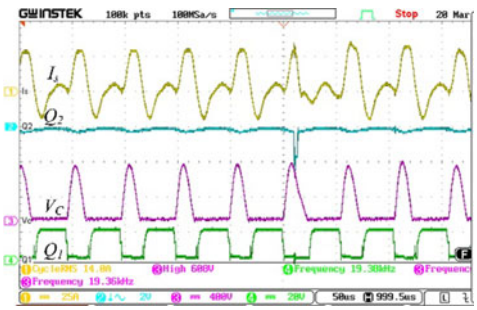

Fig. 11. Simultaneous wireless 700 W power transfer while simultaneously modulating a digit "0" by reducing the duty cycle of Q_2 from 100% to 94% (under 25 mm air gap and 0 mm offset).

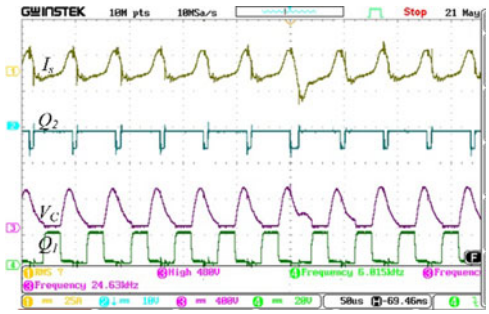

Fig. 12. Simultaneous wireless 350 W power transfer while simultaneously modulating a digit "0" by reducing the duty cycle of Q_2 from 90% to 80% (under 25 mm air gap and 0 mm offset).

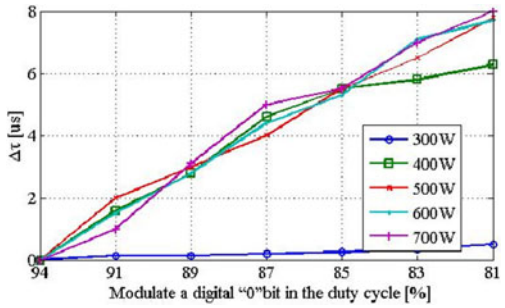

Fig. 13. Relationship between $\Delta\tau$ and duty cycle of Q_2.

transfer. Those introduce $T_Z{}'(0)$ on V_C. Figs. 10–12 reveal that the current I_s affects the operating frequency. The periods of I_s and I_p are identical, as depicted in (8). The proposed system adopts the flyback inverter, which is only constituted by ordinary electronic components with no special components; it is also small in size for convenience of installation in cars.

Fig. 13 shows the varying duty cycle of Q_2 versus $\Delta\tau$. It can be seen that after adjusting duty cycle, a near-linear relationship can be obtained for the duty cycle lies within 85% to 94% as

$$\text{Modulated } T_{\text{off}} \coloneqq \Delta\tau + \varepsilon \tag{21}$$

where the modulated T_{off} is duty off of Q_2 for the secondary unit to send the digit "0," the uncertainty $|\varepsilon| \leq 0.5\ \mu$s in the experiments. If the modulated $T_{\text{off}} + \varepsilon > \Delta$ref, the primary unit decodes data as the digit "0."

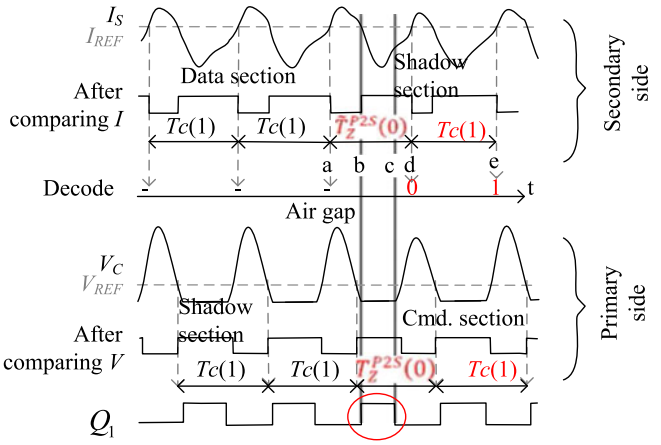

Fig. 14. Working mechanism of command transmission.

C. Command Transmission

Fig. 6 illustrates that *Tx* cmd follows *Tx* data. When the primary unit has received normal messages from the secondary unit, it reacts by sending *Tx* cmd. Fig. 14 depicts how the system handles the simultaneous wireless power transfer with the *Tx* cmd.

When the system operates normally without emergency occurred at the secondary unit, the primary unit puts command in the com. section with baud rate equal to 120 Bd as shown in Table I. The secondary unit pickups command in the shadow section from the signal "After comparing *I*." The primary unit trims the duty cycle of Q_1 when modulating a digit "0." As shown in Fig. 14, T_{ON} is shorter when modulating "0" while compared with that of modulating "1" which has longer T_{ON}. The reduced current causes a missing time $\Delta\tau$ at the primary side. Referring to Fig. 14, the primary unit sends data arranged in the Cmd. section. In the b-c section, the time of Q_1 ON is comparably shorter than other sections. The reduced current of I_p will be affecting the secondary unit. This can be referred from (24). This causes a reduced time period $\Delta\tau$ at the shadow part in the a-d section than that in the d-e section. This can be found from the upper figure of Fig. 14. The term $\Delta\tau$ generating the digital messages "0" is defined as

$$T_Z^{P2S}(0) = T_C(1) - \Delta\tau. \tag{22}$$

The secondary unit receives command and decodes it to be "0" or "1" depending on $T_C(1)$ and $\Delta\tau$. The secondary unit distinguishes the digital "0" based on the following criterion:

$$\tilde{T}_Z^{P2S}(0) < T_C(1) - \Delta\text{ref} \tag{23}$$

where Δref is a threshold for recognizing the digit "0" at the secondary side. If $\Delta\tau > \Delta$ref, the primary unit trims the duty cycle of Q_1 as

$$\text{Trimmed } T_{\text{on}} \coloneqq \Delta\tau + \varepsilon \tag{24}$$

where $\Delta\tau$ and ε are defined as above. If the modulated Trimmed $T_{\text{on}} > \Delta$ref, the secondary unit decodes data as the digit "0." Figs. 15 and 16 display the function for modulating a

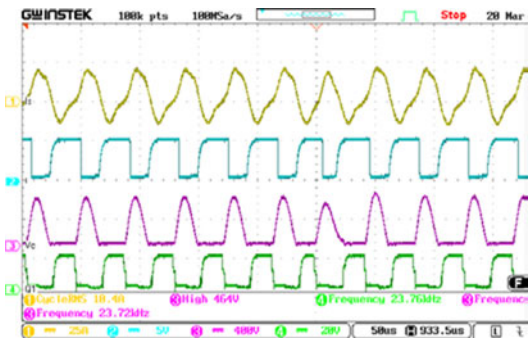

Fig. 15. Simultaneous wireless 400 W power transfer while simultaneously transferring *Tx* cmd (under 25 mm air gap and 0 mm offset).

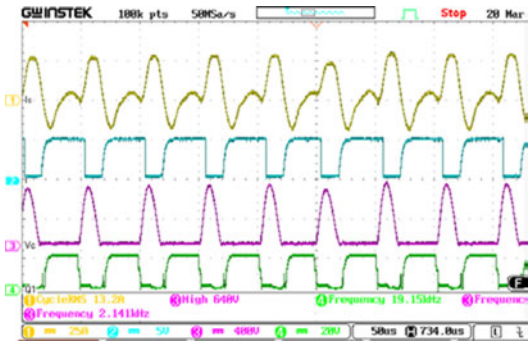

Fig. 16. Simultaneous wireless 700 W power transfer while simultaneously transferring *Tx* cmd (under 25 mm air gap and 0 mm offset).

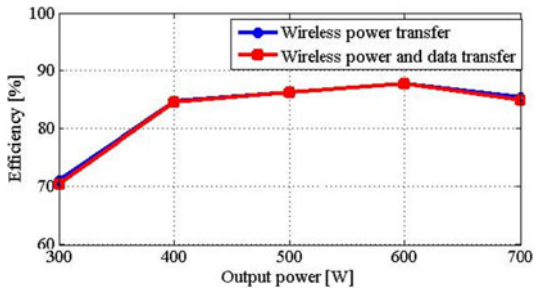

Fig. 17. Insignificant efficiency drop of the simultaneous wireless power and data transfer.

digit "0" ($\Delta\tau = 4\ \mu$s) at the center of the data string. The first to the fourth curves represents I_s, after comparing *I,* V_C, and gate voltage of Q_1. It is seen that $T_Z^{P2S}(0)$, by modulating the duty cycle of Q_1, is shorter than that of modulating a "1" by $4\ \mu$s. Figs. 15 and 16 show that the current I_p affects the operating frequency. It should be noted that the communication quality is unrelated to the duty cycle of Q_2 but to the value of $\Delta\tau$. Therefore, there is no deterioration in communication quality while using 100% or other settings of the duty cycle of Q2. However, the later would cause more power consumption because of more switching.

Degradation of the power transmission efficiency is examined when data are simultaneously transmitted with the ac power as shown in Fig. 17. In this figure, it is seen that there is only a slight

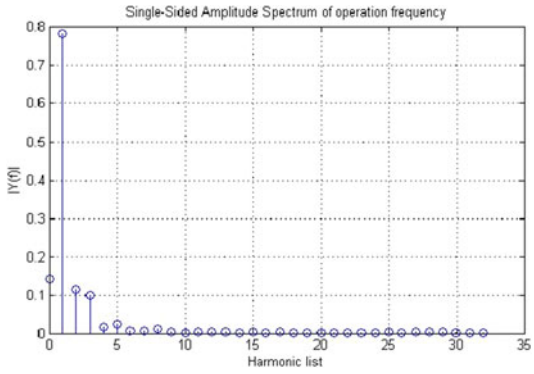

Fig. 18. Harmonics of i_s.

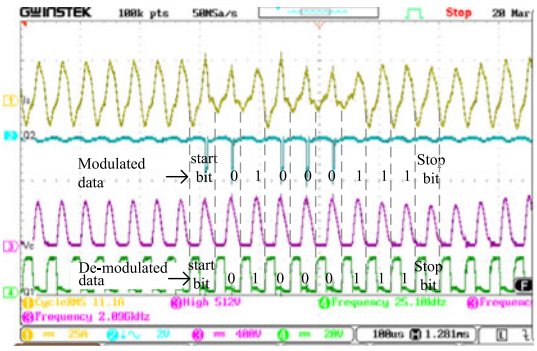

Fig. 19. Simultaneous wireless 400 W power and emergency message transfer.

change on efficiency of simultaneous power and bidirectional data transfer. Fig. 18 displays the harmonic spectrum of the secondary current i_s when the output is 600 W. In the figure, there are most significant frequency components within five order in the spectrum with THDF = 26.99%. The primary unit has a filter as shown in Fig. 1 which can filter these harmonic frequencies. In addition, the primary unit outputs power only when the load-detected function reports there is load at the secondary unit. This ensures energy will be fully transmitted to the secondary unit. Therefore, the concern of emission of high-order harmonics is not likely to exist.

D. Emergency Message

During power transfer, if there is over charging voltage or current, the system can, with the highest priority, stop transferring power immediately through emergency communication.

Experiments have been conducted by considering reduction of the duty cycle of Q_2 from 100% to 94% to induce an extra time delay $\Delta\tau = 4\ \mu$s. The results are displayed in Figs. 19 and 20. They show that when the output power is set to be low power 400 W and high power 700 W, the primary unit can decode data correctly.

E. Summary of Operation

Q_1 handles power transfer based on ZVS as illustrated in Figs. 4 and 5. Then, Q_2 sends "*Tx* data" which works with pulse

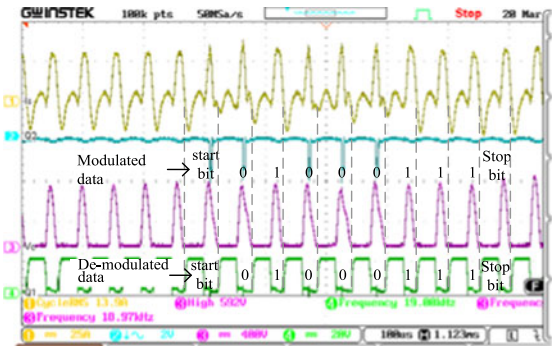

Fig. 20. Simultaneous wireless 700 W power and emergency message transfer.

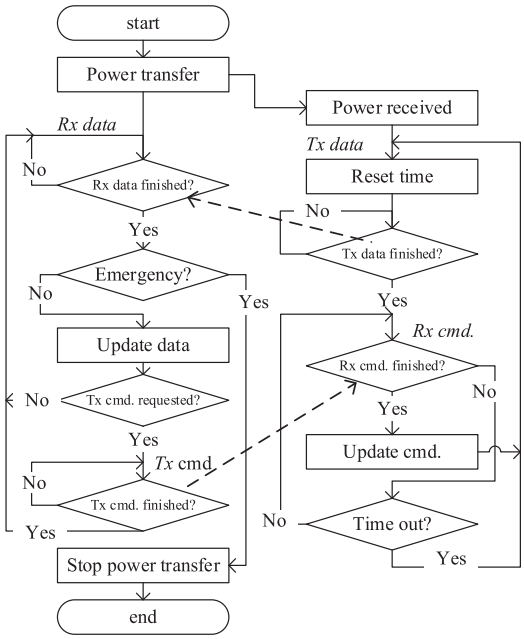

Fig. 21. Operational flow chart of the wireless power and bidirectional data transfer scheme.

weight modulation to transfer data as illustrated in Figs. 10 and 12. Next, Q_1 sends back "*Tx* cmd," see Figs. 15 and 16. If there is any contingency, such as overcharging voltage or current, the secondary unit sends an emergency message as shown in Figs. 19 and 20. Fig. 21 illustrates the operational flow of the wireless power and bidirectional data transfer scheme, which starts from time reset then proceeds to the data transmission mode. This is explained as follows:

1) Tx data: after resetting time, the secondary unit sends "Tx data" such as battery status, the vehicle identification code, or emergency message, etc., to the primary unit;
2) Rx data: the primary unit receives data;
3) Tx cmd: after the primary unit received data, it acknowledges "Tx command" which commands what type of data to be sent from the secondary unit next;
4) Rx cmd: the secondary unit receives command and conducts the corresponding action.

TABLE II
PARAMETERS AND SPECIFICATIONS OF THE PROTOTYPE IPT SYSTEM

nominal frequency	22 kHz
Max output power	700 W
Rated load	40 Ω
Primary inductance	70 μH
Primary capacitance	0.35 μF
Primary outer diameter	165 mm
Primary windings	20 turns
Mutual inductance	26.1 μH
Secondary inductance	69.4 μH
Secondary capacitance	0.35 μF
Secondary outer diameter	165 mm
Secondary windings	20 turns
L_{o1}	4 μH
L_{o2}	84 mm
C_{21}	270 μF
C_{22}	280 μF

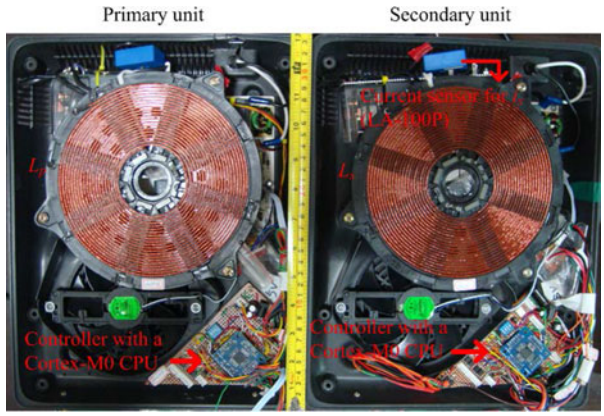

Fig. 22. Hardware of the proposed IPT system.

IV. EXPERIMENTAL VERIFICATION

Since the primary unit is operated based on ZVS, the system may change its operational frequency with the load R_L. Q_1 at the primary unit operates under ZVS to achieve higher efficiency and less switching loss. When the vertical shift of the gap between L_p and L_s or the load R_L has changed, it will cause a slight change of the operational frequency between 24 and 19 kHz. Therefore, the period of $T_C(1)$ in Figs. 4 and 5 is unlikely to be fixed. To tackle the problem, both units measure the period of $T_C(1)$ in the preamble section as a reference, as depicted in Fig. 8.

The following experiments are conducted to check whether the communication quality deteriorates when there is a shift between two power pads or a load change. Table II lists circuit parameters of the prototype IPT system. Δref is equal to $\Delta\tau/2$ in all experiments.

Hardware of the proposed system and testing scenario are shown in Figs. 22 and 23, respectively. The core of the primary and secondary control units is realized in ARM Cortex-M0 CPU to handle human–computer interaction, power transfer, and bidirectional data transmission. The operational clock of CPU is 24 MHz which is enough to meet the current requirements.

Operational flow chart of the wireless power and bidirectional data transfer scheme is shown in Fig. 21. The communication

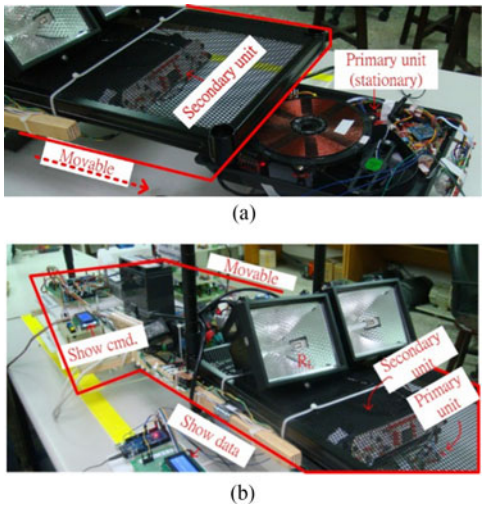

Fig. 23. Test scenario of the wireless power and bidirectional data transmission; (a) initial lateral shift between two units, and (b) vertical alignment.

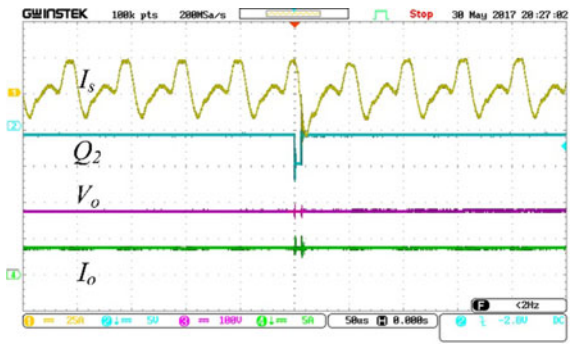

Fig. 24. Simultaneous wireless data/power transfer at 700 W when modulating a data bit with power output filtered via a second-order low-pass filter.

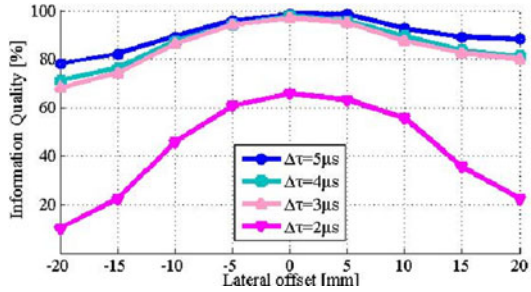

Fig. 25. Data communication quality for the different vertical shift between L_p and L_s with the nominal air gap 25 mm.

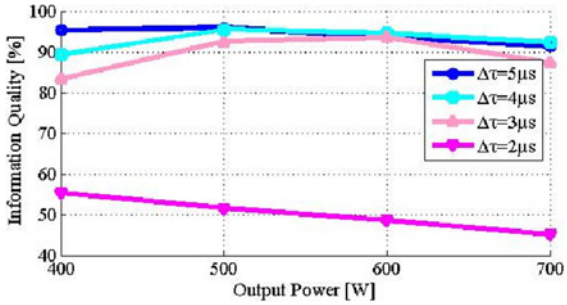

Fig. 26. Data communication quality under different output powers.

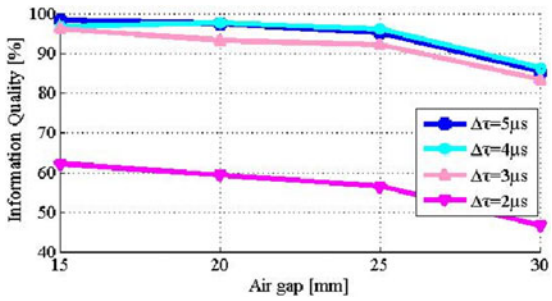

Fig. 27. Data communication quality under different air gaps between two power pads.

quality is measured by considering the index defined as

$$\text{communication quality} = \frac{\text{pass count}}{\text{total count}}\% \tag{25}$$

where total count is 1000 for the normal messages transmitted, see Fig. 6, and pass count is the number of the correct data packet received defined by

$$\text{Checksum} = \text{Data2}'\text{s}. \tag{26}$$

If checksum is equal to Data2's, the data received are recognized as correct one.

To reduce current variation during battery charge, we have included a second-order low-pass filter in the secondary side as illustrated in Fig. 1. The case of output power 700 W is shown in Fig. 24. No significant surge in current I_o and voltage V_o is seen when Q_2 modulates data.

Fig. 25 presents the result of communication quality. It was recorded by adjusting the vertical shift of the gap between L_s and L_p from –20 to +20 mm. From the experimental results, the index of improvement is observed by increasing $\Delta\tau$. Furthermore, the index can be maintained up to 90% when vertical shift of the gap remains between –5 and +5 mm and $\Delta\tau$ is kept in between 3 and 5 μs.

Fig. 26 indicates the effect of power output on communication quality. The system achieves satisfactory performance when it works between 400 and 700 W.

Concerning communication quality, Fig. 27 shows that the optimal air gap between L_s and L_p is between 15 and 25 mm. It is noted that the experimental result was obtained based on the prototype of the current design. The optimal air gap between transceiver and receiver changes with the system.

Based on the extensive results of data collected via the *LC* tank, the following polynomial related to lateral misalignment, air gap, and data collection can be established:

$$\begin{aligned} f(x,z) = {} & p_{00} + p_{10}x + p_{01}z + p_{20}x^2 + p_{11}xz + p_{02}z^2 \\ & + p_{30}x^3 + p_{21}x^2z + p_{12}xz^2 + p_{03}z^3 + p_{40}x^4 \\ & + p_{31}x^3z + p_{22}x^2z^2 + p_{13}xz^3 + p_{50}x^5 \\ & + p_{41}x^4z + p_{32}x^3z^2 + p_{23}x^2z^3 \end{aligned}$$

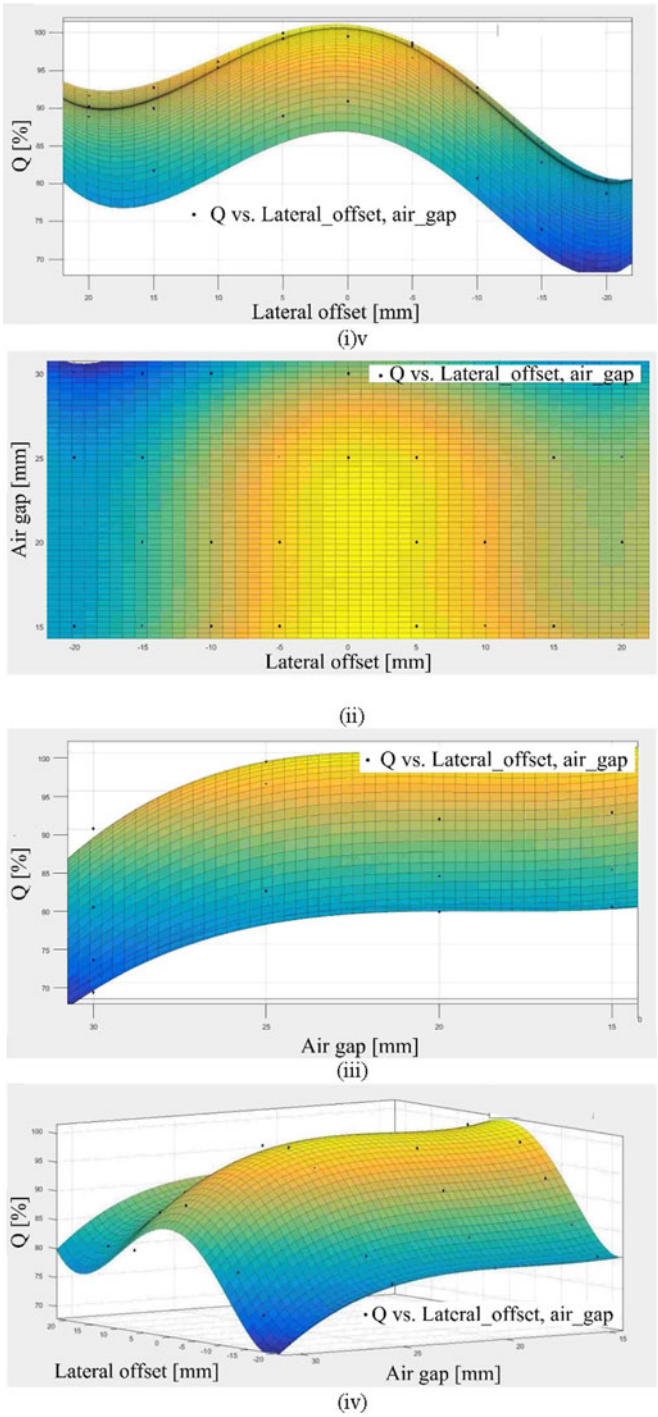

Fig. 28. Communication quality with respect to lateral misalignment and air gap; (i) lateral misalignment versus Q, (ii) lateral misalignment versus air gap, (iii) air gap versus Q, and (iv) combined lateral misalignment and air gap versus Q.

where $f(x, z)$ denotes the completely received data packet numbers which we sent per hundred times under different lateral misalignment x (mm) and air gap z (mm) within 95% confidence bounds, and $p_{00} = 177.4$, $p_{10} = 0.9575$, $p_{01} = -12.2$, $p_{20} = -0.07966$, $p_{11} = -0.1226$, $p_{02} = 0.6318$, $p_{30} = 0.001179$, $p_{21} = 0.003344$, $p_{12} = 0.005701$, $p_{03} = -0.01078$, $p_{40} = 5.342e-05$, $p_{31} = -4.097e-05$, $p_{22} = -0.0002514$, $p_{13} = -8.524e-05$, $p_{50} = -8.477e-07$, $p_{41} = 2.24e-06$, $p_{32} = 8.364e-07$, $p_{23} = 4.492e-06$.

Based on (25), the communication quality Q is computed using

$$Q = \frac{f(x, z)}{f(0, 1.0)}, \text{when } \Delta\tau = 5\ \mu\text{s}.$$

The results of data packet received and communication quality with respect to lateral misalignment and air gap are illustrated in Fig. 27. Three-dimensional plot displayed in Fig. 28(iv) shows the tendency of communication quality which can be served as the reference for positioning of the induction pads.

The weakness of the scheme considered here is less data transferring rate compared with RF communication; however, only limited data messages are needed to be transferred for the current application. Therefore, it would not severely restrict its application for the current purpose; actually, the disadvantage could be improved by introducing multiple time delays factor $\Delta\tau$. This is currently under development.

V. Conclusion

The proposed design for the IPT system for battery charging with data communication possesses the following advantages:

1) for practical and safety concerns, the primary and secondary sides can communicate bidirectionally based on the same *LC* tank resulting in a compact size of the system;
2) the controller in the primary side can control the output current to achieve steady-state compensation in the secondary side via wireless communication;
3) the speed for handling the emergency event is only 1/120 s;
4) it costs less than other RF communication. In addition, no extra signal transmission circuit (such as blue tooth, zeebee, etc.) is needed;
5) the contactless charging and discharging technology possesses the potential to be used for energy exchange between car batteries and apartment complex's energy storage tank, i.e., G2V and V2G.

References

[1] J. Dai and D. C. Ludois, "A survey of wireless power transfer and a critical comparison of inductive and capacitive coupling for small gap applications," *IEEE Trans. Power Electron.*, vol. 30, no. 11, pp. 6017–6029, Nov. 2015.
[2] H. H. Wu, G. Aaron, S. Ky, I. Paul, and M. Jeff, "A review on inductive charging for electric vehicles," in *Proc. IEEE Int. Electr. Mach. Drives Conf.*, 2011, pp. 143–147.
[3] C. S. Wang, O. H. Stielau, and G. A. Covic, "Design considerations for a contactless electric vehicle battery charger," *IEEE Trans. Ind. Electron.*, vol. 52, no. 5, pp. 1308–1314, Oct. 2005.
[4] X. Qu, H. Han, S. C. Wong, C. K. Tse, and W. Chen, "Hybrid IPT topologies with constant current or constant voltage output for battery charging applications," *IEEE Trans. Power Electron.*, vol. 30, no. 11, pp. 6329–6337, Nov. 2015.
[5] M. Budhia, J. T. Boys, G. A. Covic, and C. Y. Huang, "Development of a single-sided flux magnetic coupler for electric vehicle IPT charging systems," *IEEE Trans. Ind. Electron.*, vol. 60, no. 1, pp. 318–328, Jun. 2013.
[6] E. A. Mehdi, K. Chma, and J. Stefani, "Rapid-charge electric-vehicle stations," *IEEE Trans. Power Del.*, vol. 25, no. 3, pp. 1883–1887, Jul. 2010.

[7] C. H. Ou, H. Liang, and W. Zhuang, "Investigating wireless charging and mobility of electric vehicles on electricity market," *IEEE Trans. Ind. Electron.*, vol. 62, no. 5, pp. 3123–3133, May 2015.
[8] S. Wang, K. Izaki, I. Hirota, H. Yamashita, H. Omori, and M. Nakaoka, "Induction-heated cooking appliance using new quasi-resonant ZVS-PWM inverter with power factor correction," *IEEE Trans. Ind. Appl.*, vol. 34, no. 4, pp. 705–712, Jul./Aug. 1998.
[9] F. Sanz, C. Sagues, and S. Llorente, "Induction heating appliance with a mobile double-coil inductor," *IEEE Trans. Ind. Appl.*, vol. 51, no. 3, pp. 1945–1952, Jun. 2015.
[10] T. Diekhans and R. W. D. Doncker, "A dual-side controlled inductive power transfer system optimized for large coupling factor variations and partial load," *IEEE Trans. Power Electron.*, vol. 30, no. 11, pp. 6320–6328, Nov. 2015.
[11] U. K. Madawala, M. Neath, and D. J. Thrimawithana, "A power–frequency controller for bidirectional inductive power transfer systems," *IEEE Trans. Ind. Electron.*, vol. 60, no. 1, pp. 310–317, Jan. 2013.
[12] D. J. Thrimawithana, U. K. Madawala, and M. Neath, "A synchronization technique for bidirectional IPT systems," *IEEE Trans. Ind. Electron.*, vol. 60, no. 1, pp. 301–309, Jan. 2013.
[13] U. K. Madawala and D. J. Thrima, "A bidirectional inductive power interface for electric vehicles in V2G systems," *IEEE Trans. Ind. Electron.*, vol. 58, no. 10, pp. 4789–4796, Oct. 2011.
[14] Y. Ma, T. Houghton, A. Cruden, and D. Infield, "Modeling the benefits of vehicle-to-grid technology to a power system," *IEEE Trans. Power Syst.*, vol. 27, no. 2, pp. 1012–1020, May 2012.
[15] G. B. Joun and B. H. Cho, "An energy transmission system for an artificial heart using leakage inductance compensation of Transcutaneous transformer," *IEEE Trans. Power Electron.*, vol. 13, no. 6, pp. 1013–1022, Nov. 1998.
[16] Q. Xu, D. Hu, B. Duan, and J. He, "A fully implantable stimulator with wireless power and data transmission for experimental investigation of epidural spinal cord stimulation," *IEEE Trans. Neural Rehabil. Eng.*, vol. 23, no. 4, pp. 683–692, Jul. 2015.
[17] Y. Jang and M. M. Jovanovic, "A contactless electrical energy transmission system for portable-telephone battery chargers," *IEEE Trans. Ind. Electron.*, vol. 50, no. 3, pp. 520–527, Jun. 2003.
[18] P. Athalye, D. Maksimovic, and R. Erickson, "High-performance front-end converter for avionics applications," *IEEE Trans. Aerosp. Electron. Syst.*, vol. 39, no. 2, pp. 462–470, Apr. 2003.
[19] S. Jeong, Y. J. Jang, and D. Kum, "Economic analysis of the dynamic charging electric vehicle," *IEEE Trans. Power Electron.*, vol. 30, no. 11, pp. 6368–6377, Nov. 2015.
[20] G. R. Nagendra, L. Chen, G. A. Covic, and J. T. Boys, "Detection of EVs on IPT highways," *IEEE Emerg. Sel. Topics Power Electron.*, vol. 2, no. 3, pp. 584–597, Sep. 2014.
[21] J. Wu, C. Zhao, Z. Lin, J. Du, Y. Hu, and X. He, "Wireless power and data transfer via a common inductive link using frequency division multiplexing," *IEEE Trans. Ind. Electron.*, vol. 62, no. 12, pp. 7810–7820, Dec. 2015.
[22] T. Bieler, M. Perrottet, V. Nguyen, and Y. Perriard, "Wireless power and data transmission," *IEEE Trans. Ind. Electron.*, vol. 38, no. 5, pp. 1266–1272, Sep. 2002.
[23] S. J. Huang, T. S. Lee, and T. H. Huang, "Inductive power transfer systems for PT-based ozone-driven circuit with flexible capacity operation and frequency-tracking mechanism," *IEEE Trans. Ind. Electron.*, vol. 61, no. 12, pp. 6691–6699, Dec. 2014.
[24] X. Qu, W. Zhang, S. C. Wong, and C. K. Tse, "Design of a current-source-output inductive power transfer LED lighting system," *IEEE Emerg. Sel. Topics Power Electron.*, vol. 3, no. 1, pp. 306–314, Mar. 2015.
[25] A. Abdolkhani and A. P. Hu, "Improved coupling design of contactless slip ring for rotary applications," *IEEE Emerg. Sel. Topics Power Electron.*, vol. 3, no. 1, pp. 288–295, Mar. 2015.
[26] X. Ju, L. Dong, X. Huang, and X. Liao, "Switching technique for inductive power transfer at high-Q regimes," *IEEE Trans. Ind. Electron.*, vol. 62, no. 4, pp. 2164–2173, Apr. 2015.
[27] Z. H. Wang, Y. P. Li, Y. Sun, C. S. Tang, and X. Lv, "Load detection model of voltage-fed inductive power transfer system," *IEEE Trans. Power Electron.*, vol. 28, no. 11, pp. 5233–5243, Nov. 2013.
[28] I. Sheikhian, N. Kaminski, S. Vob, W. Scholz, and E. Herweg, "Optimisation of the reverse conducting IGBT for zero-voltage switching applications such as induction cookers," *IET Circuits Devices Circuits Syst.*, vol. 8, no. 3, pp. 176–181, Nov. 2013.
[29] C. S. Wang, G. A. Covic, and O. H. Stielau, "Power transfer capability and bifurcation phenomena of loosely coupled inductive power transfer system," *IEEE Trans. Ind. Electron.*, vol. 51, no. 1, pp. 148–157, Feb. 2004.
[30] W. D. Stanley and J. M Jeffords, *Electronic Communications: Principles and Systems*. Boston, MA, USA: Delmar Cengage Learning, 2005.

Chih-Cheng Huang was born in Taichung, Taiwan, R.O.C., in 1970. He received the M.S. and Ph.D. degrees in electrical engineering from the National Chung Hsing University, Taichung, Taiwan, R.O.C., in 2012 and 2017, respectively.

His research interests include industrial electronics, optimization techniques in power system economics, and related applications.

Chun-Liang Lin (SM'02) was born in Tainan, Taiwan, R.O.C., in 1958. He received the Ph.D. degree in aeronautical and astronautical engineering from the National Cheng Kung University, Tainan, Taiwan, R.O.C., in 1991.

From 1995 to 2003, he was, respectively, an Associate Professor and a Professor in the Department of Automatic Control Engineering, Feng Chia University, Taichung, Taiwan, R.O.C. Currently, he is the Chair Professor in the Department of Electrical Engineering, National Chung Hsing University, Taichung, Taiwan, R.O.C. His research interests include guidance and control, intelligent control, network control, and synthetic biology.

Dr. Lin was the Chair of IEEE Control Systems Society, Taipei Chapter from 2012 to 2015. He has also been a member of board of governors, IEEE Taipei Section since 2015. He received the Distinguished Research Award three times from the National Science Council of Taiwan in 2000, 2003, and 2010.